Under Three-Dimensional Oscillatory Conditions," *AGARDograph 117*, Butterworth Publications Ltd., London, England, 1967.

[4] Smith, A. J. et al., "The Sensitive Time Lag Theory and Its Application to Liquid Rocket Combustion Instability Problems," AFRPL-TR-67-314, March 1968, Vol. I, Aerojet-General Corp., Sacramento, Calif.

[5] Zinn, B. T. and Savell, C. T., "A Theoretical Study of Three-Dimensional Combustion Instability in Liquid-Propellant Rocket Engines," *Twelfth Symposium (International) on Combustion*, Combustion Inst., Pittsburgh, Pa., 1968, pp. 139–147.

[6] Crocco, L., Monti, R., and Grey, J., "Verification of Nozzle Admittance Theory by Direct Measurement of the Admittance Parameter," *ARS Journal*, Vol. 31, 1961, p. 771.

[7] Buffum, F. G., Dehority, G. L., Slates, R. O., and Price, E. W., "Acoustic Losses of a Subscale Cold-Flow Rocket Motor for Various 'J' Values," Technical Publication 3932, 1966, Naval Ordnance Test Station, China Lake, Calif.

[8] Culick, F. E. C. and Dehority, G. L., "Analysis of Acoustic Waves in a Cold-Flow Rocket," *Journal of Spacecraft and Rockets*, Vol. 6, No. 5, May 1969, pp. 591–595.

[9] Scott, R. A., "An Apparatus for Accurate Measurement of the Acoustic Impedance of Sound Absorbing Materials," *Proceedings of the Physical Society*, Vol. 58, 1946, p. 253.

[10] Lippert, W. K. R., "The Practical Representation of Standing Waves in an Acoustic Impedance Tube," *Acoustica*, Vol. 3, 1953, p. 153.

[11] Morse, P. M. and Ingard, K. U., *Theoretical Acoustics*, McGraw-Hill, New York, 1968, Chaps. 9 and 11.

[12] Bell, W. A., "Experimental Determination of Three-Dimensional Liquid Rocket Nozzle Admittances," Ph.D. thesis, 1972, Georgia Inst. of Technology, Atlanta, Ga.

[13] Gately, W. S. and Cohen, R., "Methods for Evaluating the Performance of Small Acoustic Filters," *Journal of the Acoustical Society of America*, Vol. 46, 1969, p. 6.

[14] Pfahl, R. C. and Mitchel, B. J., "Nonlinear Regression Methods for Simultaneous Property Measurement," *AIAA Journal*, Vol. 8, 1970, p. 1046.

[15] Marquardt, D. W., "An Algorithm for Least-Squares Estimation of Nonlinear Parameters," *Journal of the Society for Industrial and Applied Mathematics*, Vol. 11, June 1963, p. 431.

MARCH 1973 AIAA JOURNAL VOL. 11, NO. 3

Ultraviolet Radiation from the Bow Shock of a Sphere during Atmospheric Re-Entry

LEONILDA A. FARROW* AND ARTHUR H. FITCH*
Bell Laboratories, Murray Hill, N.J.

Onboard measurements of the ultraviolet radiation at 2710Å from the bow shock of a re-entry sphere have been compared with predictions based on a nonequilibrium calculation which couples the thermodynamics and fluid dynamics of the gas with the chemical kinetics. The agreement is found to be good at altitudes from 100 kft to 250 kft, whereas a previous equilibrium calculation gave poor agreement at all altitudes. The main contribution to the radiation at 2710Å is found to come from the NO β and γ bands. The correction to the equilibrium calculation comes from the finding that the NO concentration calculated at equilibrium and calculated dynamically can differ as much as 3 orders of magnitude. The motion of the sphere during re-entry is also found to have an important effect on the final results.

Introduction

THE intensity of ultraviolet radiation generated by a blunt body during atmospheric re-entry at suborbital velocities, although of considerable importance in re-entry physics, is a topic on which relatively little theoretical or experimental work has been done. Because of the very strong absorption by atmospheric ozone, the middle ultraviolet radiation emanating from the bow shock of a blunt-nosed re-entry vehicle can be measured only by instruments carried on board the vehicle. Two flights of the Bell Sphere Program, B–08 and B–13, carried radiometers designed to provide an absolute measurement of the ultraviolet intensity at 2710Å as a function of altitude during re-entry.

Presented as Paper 72-692 at the AIAA 5th Fluid and Plasma Dynamics Conference, Boston, Mass., June 26–28, 1972; submitted July 10, 1972; revision received October 16, 1972. It is a pleasure to acknowledge the cooperation of R. F. Bergeron Jr., R. M. Lum, and K. B. McAfee Jr.

Index categories: Re-Entry Vehicle Testing; Thermochemistry and Chemical Kinetics.

* Member of Technical Staff, Department of Atmospheric Research.

The radiation in this region comes principally from three sources.[1] The first is the transition in the oxygen molecule from the $^3\Sigma_u^-$ state to the $^3\Sigma_g^-$ ground state.[2] The second and third are the β and γ bands of NO; these are due respectively to the $B^2\Pi \rightarrow X^2\Pi$ (ground state) and $A^2\Sigma^+ \rightarrow X^2\Pi$ transitions.[2] The cross sections for this radiation are found to be strongly temperature-dependent[1]; therefore the total radiation coming from the bow shock is a function of temperature and of the concentration in the bow shock of O_2 and NO. A previous evaluation based on equilibrium concentrations at a given temperature has been found to be in poor agreement with the experimental data at all altitudes. Subsequently, however, techniques have been developed that make possible a chemical kinetic calculation in the bow shock which fully couples the chemical kinetics to the thermodynamics and fluid dynamics. The results of such a description of the bow shock show that, at a given temperature, the amount of O_2 is negligible, eliminating the Schumann-Runge contribution, and the NO concentration can be as much as three orders of magnitude higher than that found in the equilibrium concentration. This correction to the contribution from the β and γ bands brings the calculated values into good agreement with the experimental values.

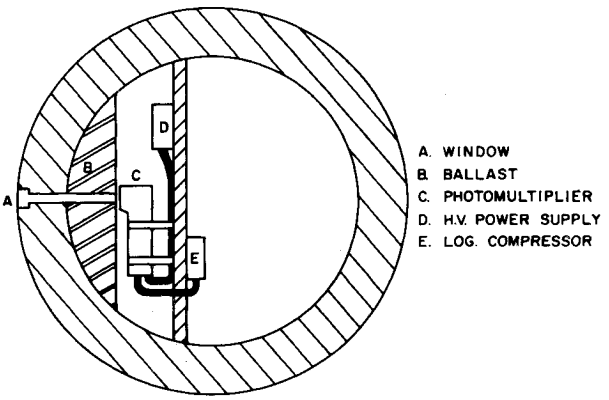

Fig. 1 Schematic of B–08 experiment.

Experimental Results

Flight B–08 carried an ultraviolet radiometer shown semi-schematically in Fig. 1. An EMR solarblind photomultiplier, Type 6414–08–18B, received radiation from the bow shock region through a light pipe in the bow of the sphere. A window of ultraviolet-grade fused quartz protected the photomultiplier and its ultraviolet filter from the extreme pressures generated during re-entry. Instrumentation and calibration details are included in Appendix A.

Figure 2 shows the experimental results obtained from flight B–08, along with the results of an equilibrium calculation which is discussed in the next section, and the results of the present nonequilibrium calculation at altitudes 100, 130, 225, and 250 kft. The dashed line indicates the period during which saturation of the radiometer occurred, corresponding approximately to the altitude regime from 220 kft to 130 kft. Errors on the experimental points are estimated at 50%. It should be noted that the photomultiplier window is not looking simply into the stagnation point. The ripples in the observed radiance on the high-altitude side of the curve in Fig. 2 are due to oscillations of the sphere, and to the possible coning motion as well.

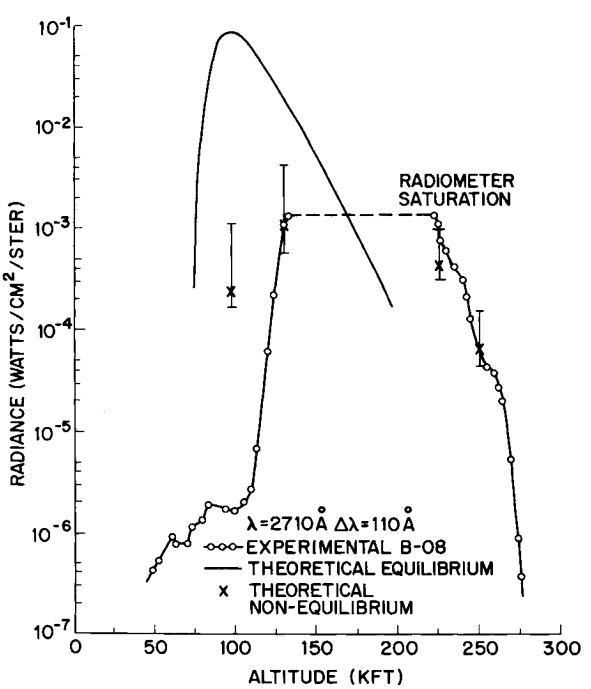

Fig. 2 Experimental results from flight B–08 together with the results of an equilibrium calculation and the results of the nonequilibrium calculation described in this paper.

O_2	+ O_2	→	O	+ O	+	O_2
O_2	+ N_2	→	O	+ O	+	N_2
O_2	+ O	→	O	+ O	+	O
O_2	+ N	→	O	+ O	+	N
O_2	+ NO	→	O	+ O	+	NO
N_2	+ O_2	→	N	+ N	+	O_2
N_2	+ N_2	→	N	+ N	+	N_2
N_2	+ O	→	N	+ N	+	O
N_2	+ N	→	N	+ N	+	N
N_2	+ NO	→	N	+ N	+	NO
NO	+ O_2	→	O	+ N	+	O_2
NO	+ N_2	→	O	+ N	+	N_2
NO	+ O	→	O	+ N	+	O
NO	+ N	→	O	+ N	+	N
NO	+ NO	→	O	+ N	+	NO
O	+ NO	→	N	+ O_2		
O	+ N_2	→	N	+ NO		
O	+ N	→	NO^+	+ e^-		
e^-	+ O_2 + O_2	→	O_2^-	+ O_2		
e^-	+ O_2 + N_2	→	O_2^-	+ N_2		

Fig. 3 The 20 chemical reactions which, along with the 20 reverse reactions of those shown, form the 40 reactions which are used as a basis for calculating the chemical kinetics of the bow shock.

Source of Ultraviolet Radiation

The basis for the chemical kinetics of the bow shock region is a set of 40 chemical equations,[3] 20 of which are shown in Fig. 3; the remaining 20 are the reverse of those in Fig. 3. The species involved are O_2, O, N_2, N, NO, NO^+, electrons, and O_2^-. This set of equations is suitable for a region such as the bow shock where temperatures are high and the dissociation reactions of the first 14 equations are important.

Each equation has associated with it a reaction rate K which is a function of the temperature T according to the general form of the Arrhenius equation

$$K = AT^B e^{-c/T} \tag{1}$$

The constants A, B, and c for each reaction of Fig. 3 are known[4] to within a factor of 3 for temperatures up to 5000°K. As will be seen, the temperatures in a very thin layer just inside the bow shock are considerably higher than this, and Eq. (1) was extrapolated with unknown error. However, in that part of the shock contributing most of the ultraviolet radiation, temperatures range between 1000 and 9000°K, closer to the measured range.

Breene and Nardone[1] have calculated the radiation emission from heated air at equilibrium; of the species used in the equations of Fig. 3, they have considered the first positive bands ($B^3\Pi \rightarrow A^3\Sigma_u^+$) and second positive bands ($C^3\Pi_u \rightarrow B^3\Pi_g$) of N_2, the γ bands ($A^2\Sigma^+ \rightarrow X^2\Pi$) and β bands ($B^2\Pi \rightarrow X^2\Pi$) of NO, and the Schumann-Runge bands ($B^3\Sigma_u^- \rightarrow X^3\Sigma_g^-$) of O_2. At 2710Å, their calculations show that the N_2 contributions are

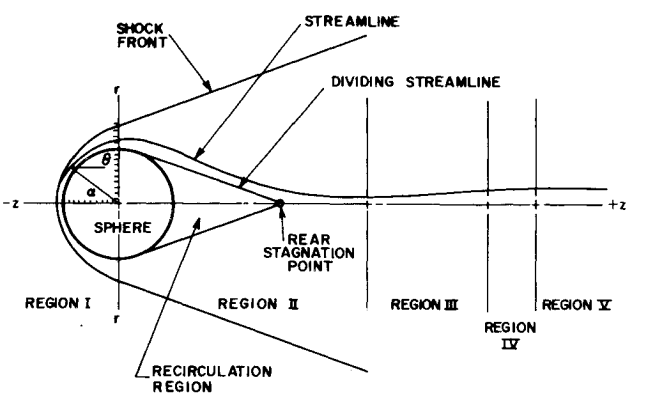

Fig. 4 Schematic diagram, not necessarily to scale, of the bow shock and near and far wakes; θ is the flow angle, z and r the Cartesian coordinates; z is normalized with respect to the sphere radius, is zero at the sphere's center, and positive to the right of the r axis; α is the angle of oscillation.

negligible. As will be discussed subsequently, the composition of the hot nonequilibrium gas is such that the Schumann-Runge contribution is also negligible in this case, leaving NO as the sole source of radiation.

The details of the nonequilibrium calculation, which couples chemical kinetics with thermodynamics and inviscid fluid dynamics, are presented in Appendix B. This calculation was done along one streamline, which is shown schematically in Fig. 4. Initial conditions at the shock front were derived at each altitude considered from the Rankine-Hugoniot relations[5] based on conservation of mass, energy, and momentum across the shock front. The calculation was then carried out at five altitudes: 100, 130, 175, 225, and 250 kft.

Figure 5 shows the results at 175 kft for a 15-in. diameter sphere traveling at a velocity of 21.75 kft/sec. The evolution of all species concentrations save O_2^-, which is always negligible, is shown. Also appearing on the horizontal axis at their corresponding times are the values of z shown in Fig. 4. These values of z are normalized to the sphere radius, with the origin at the center of the sphere. Total density is also included, as is absolute temperature T, with its scale on the right vertical axis.

The evolution of the species can be readily understood by considering the chemistry of Fig. 3 in conjunction with thermodynamic laws. Initial temperature is very high at approximately 20,000°K, which is nearly 2 ev. Note that the total density and the temperature remain roughly constant for nearly 0.1 μsec. Then the temperature begins to fall as energy goes into dissociation of O_2, and total density begins to rise. Even though temperature continues to fall, total density peaks at about 20 μsec and begins to fall; this occurs because pressure is falling rapidly in this region.

At very early times, in the first 10^{-10} sec, atomic oxygen has already risen from nothing to a concentration of more than 10^{13} cm^{-3}, whereas atomic nitrogen does not reach this level until 10^{-8} sec. This is due solely to the greater rate for dissociation of O_2. This can be confirmed by realization that the dissociation energy for O_2 is 5 ev as compared to nearly 10 ev for N_2.

NO first reaches the 10^{13} cm^{-3} concentration at 10^{-8} sec because of the reaction

$$O + N_2 \rightarrow N + NO \tag{2}$$

and the sufficiency of atomic oxygen. NO shows a slight peak at 0.1 μsec and then drops slightly as the O begins to level off. However, NO begins to rise again just below 1 μsec and peaks strongly at 10 μsec. This peaking follows the rise in N because of the reaction

$$N + O_2 \rightarrow O + NO \tag{3}$$

Also, as the temperature drops, some recombination of N and O to form NO is beginning to take place.

Electrons reach the 10^{13} level between 0.1 and 1 μsec because of the reaction

$$O + N \rightarrow NO^+ + e \tag{4}$$

which is important at this time because of the abundance of O and N. The curve for electrons is identical with that for NO^+ because of charge conservation and the negligible amount of O_2^-. Note that the total density and therefore all species concentrations drop as a result of the pressure drop, illustrating the importance to the chemical kinetics of the coupling to thermodynamic properties.

Just below 1 μsec, the concentration of O_2 drops below 10^{13} cm^{-3} and continues to fall for the entire bow shock region. It should be noted that the first μsec corresponds to the reactions taking place in a very thin, hot region just inside the shock front, as can be seen from the fact that $z = 1$ on the streamline occurs just after 1 μsec. Therefore in nearly all the shock region, the amount of O_2 is many orders of magnitude below the amount of NO. Thus the contribution to total ultraviolet radiation in the observed region from the Schumann-Runge bands proves to be negligible compared to the contribution from the NO β and γ bands. This result holds for all other altitudes studied.

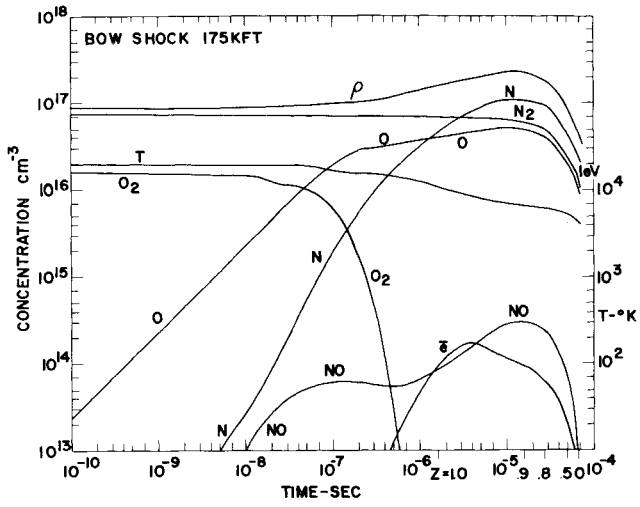

Fig. 5 Concentration of the eight species of Fig. 3 vs time along a streamline; also included are the total number density ρ, and the temperature T referred to the scale on the right-hand vertical axis; appearing on the horizontal axis at their corresponding times are the values of z shown in Fig. 4.

The absolute amounts of radiation calculated by Breene and Nardone[1] depend on the absolute values of species concentration calculated by Gilmore[6] for equilibrium heated air, as well as on temperature and density. The amount of radiation to be expected from the bow shock based on this equilibrium calculation is shown in Fig. 2 and obviously is in poor agreement with the experimental data at all altitudes. This poor agreement occurs mainly because the concentration of NO at equilibrium is markedly different from the NO concentration of the fully coupled calculation. This is so because an equilibrium calculation would allow sufficient time to elapse for the back reactions to balance the forward reactions at a given temperature. For the rates in use here, this equilibrium time is much longer than the total transit time along the streamline in the bow shock.

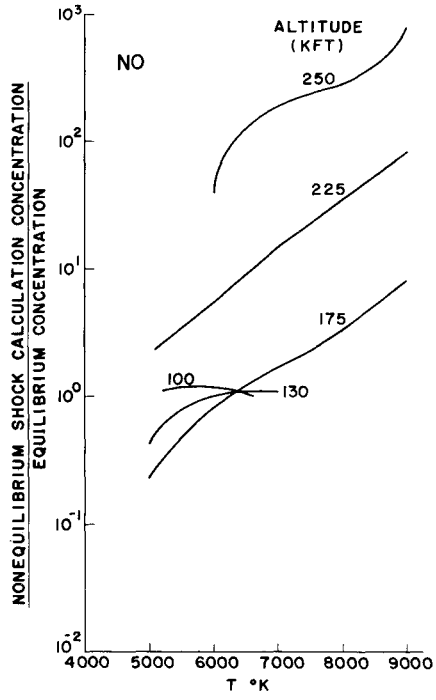

Fig. 6 The ratio of the nonequilibrium to the equilibrium density of NO vs temperature along the streamline at each altitude.

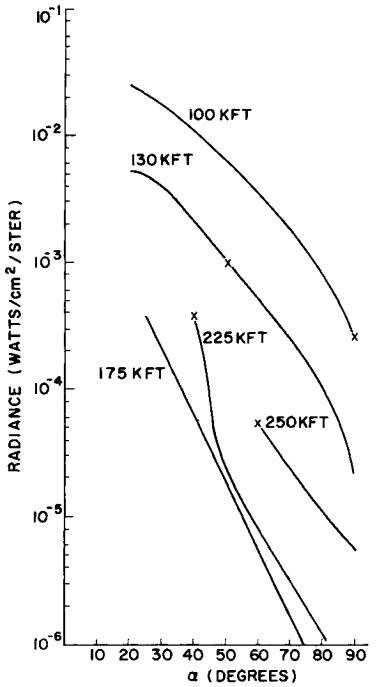

Fig. 7 Calculated radiance from the bow shock at 2710Å as a function of the angle α (see Fig. 4); at each altitude the point of best agreement with the experimental data is marked with a cross.

Figure 5, which is calculated at 175 kft, is typical for the nonequilibrium calculation at all altitudes considered, and the ratio of the nonequilibrium to the equilibrium value of NO is plotted in Fig. 6 as a function of temperature for all altitudes. The ratio can be as high as 1000 at 250 kft, and correspondingly lower at lower altitudes.

Note that the curves of Fig. 6 for the lower altitudes do not show the same drop in the ratio with decreasing temperature as do the three higher altitudes. This anomalous behavior may be due to the fact that, as explained in Appendix B, both the pressure field and the streamline shape were not calculated along with the chemical kinetics, but were derived from a more complicated two-dimensional calculation.[7]

The equilibrium values calculated by Breene and Nardone[1] may now be corrected by multiplying by the appropriate ratio of Fig. 6. Whereas their absolute units are in w/cm^3-sterad-μ, the experimental results are in w/cm^2-sterad. If the ultraviolet filter is assumed to have a gaussian shape with half-power width 100Å, then it adds a factor of $0.0012(\pi)^{1/2}$ μ.

It remains to multiply by the shock thickness, which is a function of the angle of oscillation α, as shown in Fig. 4. As can be seen in Figs. 5 and 6, temperature, NO ratio, and therefore total radiation emitted depend on z, or alternately upon α. Figure 7 shows this dependence of the total radiation as a function of α for each altitude. Thus the variation for a single altitude can differ by as much as 2 to 3 orders of magnitude. It should be stressed that these results were derived from fully coupled calculations on only one streamline. However, according to the inviscid CAL calculations at 175 kft (Appendix B), these results are good to 20% along a given angle α except for the very thin, very hot layer at the edge of the shock itself. This particular streamline did not descend below 20°; in any case that part of the shock below 15° is not attempted by the CAL code[7] and therefore could not be attempted here. The 225 and 250 kft curves start at 40° and 60°, respectively, because at lower values the temperatures are greater than the 9000°K maximum employed by Breene and Nardone.[1]

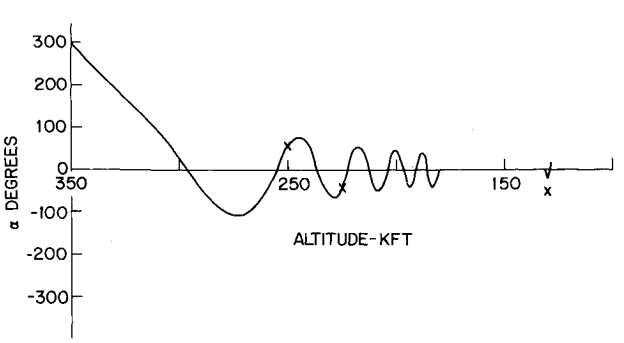

Fig. 8 Numerical solution of the equation of motion for the sphere as it re-enters the atmosphere; at each of the altitudes shown in Fig. 9, the corresponding best fit angle is marked with a cross.

On four of the altitude curves shown in Fig. 7, there is marked a point corresponding to best agreement with the experimental results of Fig. 2. Because the radiometer was saturated at 175 kft, no point has been indicated for this altitude in Fig. 7. This difficulty will be discussed shortly.

There are no direct experimental measurements of α as a function of altitude; all that is available is the initial angular velocity of the sphere at 350 kft, at which point the atmosphere begins to have an effect on its motion. If it is assumed that all motion takes place in a plane, the motion can be described by the equation of a large angle pendulum with a variable gravity depending on the density of the atmosphere. Since this is a second-order differential equation, the angle itself at 350 kft must be known before the equation can be solved. Since α at 350 kft is not known experimentally, the equation has been solved for various initial values of α and the results for α = 300° are shown in Fig. 8. Also marked are the angles necessary for good agreement with the experimental values of Fig. 2 at 250, 225, and 130 kft. Oscillations become so rapid below 175 kft (a period of 0.7 sec at 175 kft) that only a portion has been drawn at 130 kft, and no attempt has been made at 100 kft. Agreement is good at the higher altitudes, but the amplitude is too small at the lower altitudes, indicating that the simple planar motion no longer holds at greater atmospheric density.[9]

The final calculated values of radiation are plotted in Fig. 2. The errors are due mainly to using just one streamline (±20%) and to the uncertainty in the oscillator strengths used to calculate the NO radiation, which are estimated[1] to be a factor of 3 higher, leading to the error asymmetry shown. The large errors at the two lower altitudes are due to uncertainty in the proper value of α, as shown in Fig. 8. As for the saturated region, note from Fig. 8 that below 225 kft α is approaching zero, the region of maximum temperature and radiation. Obviously this amount of radiation saturates the instrument and, apparently, it cannot recover sufficiently rapidly despite the oscillations to larger angle indicated in Fig. 8. There are no laboratory measurements on the instrument which either oppose or corroborate this explanation.

A word should be said about the possibility of reabsorption in the 3-cm path between the window and the filter, which is placed in front of the photomultiplier (Fig. 1). This can be estimated by realizing that the temperature at the filter must be of the order of 300°K to prevent the filter from melting. If some equilibrium distribution is assumed for the temperature between the filter and the bow shock at the surface of the sphere, the resulting amount of ozone can be calculated. The reabsorption due to this ozone is negligible.

Conclusion

The measurement of the ultraviolet radiation at 2710Å coming from the hot gas in the bow shock of a sphere re-entering the Earth's atmosphere has been made possible by mounting a radiometer and associated equipment onboard such a sphere and looking right into the shock region during the re-entry period. A calculation of the expected radiation from strictly equilibrium considerations only gives very poor agree-

ment everywhere with the experimental data. Improvement in the agreement can be obtained by using a nonequilibrium fully-coupled calculation and by including the effects of the oscillatory motion of the sphere during re-entry. The difficulties encountered in interpreting the results suggest that any future experimental studies of heated air around re-entry vehicles should include some method of monitoring the angle α throughout re-entry and a careful study of the saturation recovery time of the radiometer. The dynamic calculations should also include more streamlines so that the properties of the bow shock may be mapped out in more detail.

Appendix A: Instrumentation and Calibration

The radiometers carried in several of the flights in the re-entry sphere program were designed to detect radiation in a narrow interval at a number of selected wavelengths. One of these radiometers, designed for operation at 2710Å and described here, was typical of many radiometers flown in the Sphere Program. The bow shock radiation generated during re-entry was split between the 2710Å radiometer and a similar radiometer designed for operation at a different wavelength by a beam-splitting mirror.

An over-all view of the optical layout of the ultraviolet radiometers is shown in Fig. 9. A window of ultraviolet-grade fused silica protects the radiometers from the excessive pressures generated during re-entry. Wide-angle scattering of the bow shock radiation is minimized by threading the 0.125-in.-diam hole and by the series of blackened baffles shown in Fig. 9.

The filters used in the two ultraviolet channels are multilayer interference filters obtained from the Thin Film Division of Infrared Industries. The filters had a diameter of 0.75 in. and are mounted in the forward end of the phenylfiber diode housings. The bandpass curve for the 2710Å filter is shown in Fig. 10.

The detector for the 2710Å radiometer was an IT & T photodiode, Type FW-140. The FW-140 is a semiminiaturized high-vacuum photodiode with a sapphire window and a cesium telluride photocathode. Dark currents of these diodes were checked over a period of several months and the values obtained were typically in the 10^{-12} amp range. The photocurrents from the diode detectors were fed into logarithmic amplifiers capable of compressing input currents over a 10^{-5} to 10^{-10} amp range into a 0 to 5 volt output. These amplifiers, a modular type, standard on many experiments in the Bell Sphere program, were supplied by Washington Technological Associates.

The power in watts in the wavelength interval $\Delta\lambda$ incident upon the detector from a diffuse source is given by

$$P_D = H_D A\Omega(\Delta\lambda)\tau_{\max} \tag{A1}$$

where H_D = radiance of the diffuse source (w/cm^2-sterad-mμ),

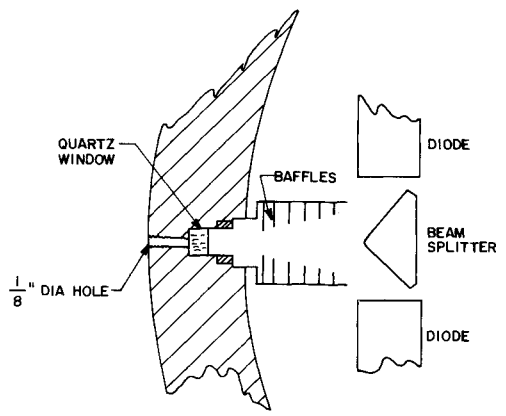

Fig. 9 Optical layout of experiment.

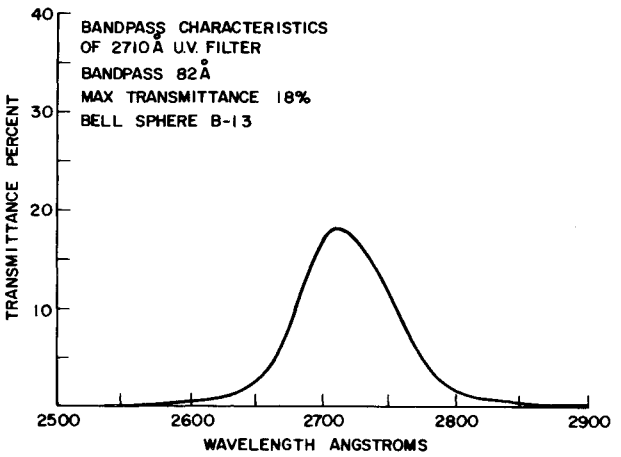

Fig. 10 Bandpass characteristics of 2710Å filter.

A = area of the aperture (cm^2), Ω = field of view of the radiometer (steradians), and $\tau_{\max}$ = maximum transmittance of the bandpass filter.

The power incident on the detector from a standard point source is given by

$$P_p = H_p A(\Delta\lambda)\tau_{\max} \tag{A2}$$

where H_p = the irradiance produced by the point source at the aperture of the radiometer (w/cm^2-mμ).

The quantum efficiency, expressed, say, in amp per watt, is independent of whether the radiation received by the detector comes from a diffuse or a point source. This yields

$$I_D/H_D A\Omega(\Delta\lambda)\tau_{\max} = I_p/H_p A(\Delta\lambda)\tau_{\max} \tag{A3}$$

or

$$I_D/H_D\Omega = I_p/H_p \tag{A4}$$

Using both a diffuse and a standard point source, the equality expressed in Eq. (A4) has been verified experimentally. The current I_p produced during re-entry is obtained from analog recordings of the output voltage of the logarithmic compression amplifiers. The relationship between these two quantities has been determined by the amplifier calibration. Rewriting Eq. (A4) yields the basic equation for the radiometer calibration

$$H_D = (H_p/I_p\Omega)I_D \tag{A5}$$

With a known radiance H_p produced by a standard point source, the output current I_p is measured in the preflight calibrations.

The radiometer characteristics and the results of the preflight calibrations are summarized in Table 1.

Appendix B: The Bow Shock Calculation

For the usual chemical kinetics problem at constant pressure and temperature, the chemical equations of Fig. 3 are transformed to eight differential equations, one for each species.

If temperature and pressure are not constant, so that density is changing, and if it is assumed that the density of each species

Table 1 Radiometer characteristics

Center wavelength of radiometer	2710Å
Solid angular field of view, Ω	1.04×10^{-2} sterad
H_p	8.48×10^{-8} w/cm^2-mμ
I_p	9.6×10^{-11} amp
$H_p/I_p\Omega$	8.48×10^4 w/amp / cm^2-mμ-sterad

changes in the same manner as the total, it is necessary to add to the right-hand side of each equation a term of the form $(1/\rho)(d\rho/dt)V(I)$, where $V(I)$ is the concentration of the Ith species. In the streamtube problem, temperature and density are not known but must be calculated along with the concentrations, as follows.

Thermodynamic variables are pressure p, temperature T, mass density ρ (alternatively, number density N), and static enthalpy h. Along the streamtube, the velocity u must also be considered. The geometry of the streamline can be given by the Cartesian coordinates z and r (see Fig. 4) or by the flow angle θ, such that $dr/dz = \tan\theta$. This gives a total of six variables in addition to the chemical species.

Figure 4 is a schematic diagram of a typical streamline starting at the bow shock boundary and ending in the far wake. Steady laminar flow is described in Regions I–IV; turbulent flow starts in Region V. Each region is characterized by slightly different physical conditions. (There is a precursor region in front of the bow shock, but it will not be considered in this paper.)

Four equations are immediately available and are applicable in all regions having laminar flow, from the bow shock up to, but not including, the turbulent far wake. These are

$$p = NkT \tag{B1}$$

$$h + \tfrac{1}{2}u^2 = \text{const} \tag{B2}$$

$$u\,du = -\,dp/\rho \tag{B3}$$

$$h = \bar{c}_p T + \sum_i c_i \Delta h_i(0) \tag{B4}$$

Equation (B1) is the usual perfect gas-law equation of state, where k is Boltzmann's constant. Equation (B2) is just the conservation of energy applied to the present conditions. Equation (B3) is Bernoulli's equation, or conservation of momentum. Equation (B4) is the caloric equation of state, and requires some further discussion.

The quantity $\bar{c}_p$ is a weighted average of the specific heats of the chemical species involved (eight in this case). Thus

$$\bar{c}_p = \sum_i c_i c_{p_i} \tag{B5}$$

where c_i is the mass fraction of species i, and c_{p_i} the specific heat of species i. In Eq. (B4), the expression $\Delta h_i(0)$ is the enthalpy of formation of species i at 0°K. The quantities c_{p_i} and $\Delta h_i(0)$ have been measured experimentally[10] for the eight species.

Two more equations are needed, and these were obtained in the bow shock region with the aid of the bow shock calculation made by the Cornell Aeronautical Laboratory[7] (CAL). The CAL code contains a chemistry similar to that of Fig. 3 and will calculate species concentrations, pressure, density, temperature, enthalpy, and velocity as a function of position in two dimensions, as well as give the shape of the shock front. Although these results meet all requirements, there are certain disadvantages to this code. For one, the running time is very long, up to 45 min on an IBM 360/85. In addition, there are convergence problems for some cases of interest, particularly small spheres at low altitudes. For example, it is difficult to obtain convergence for a 15 in. diameter sphere below 175 kft at a vehicle (freestream) velocity of 21.75 kft/sec. Finally, the chemistry is fixed in the program and cannot be changed. Nevertheless, the results of this excellent code provided an indispensible starting point for simpler but more flexible and economical calculations.

The CAL results for the velocity field may be used to find a streamline from the fundamental equation

$$dy/dx = v_y/v_x \tag{B6}$$

The CAL results are also used to obtain the final needed equation. The pressure field, normalized to the quantity $\rho_0 v_0^2$ (where v_0 is the freestream velocity and ρ_0 is the ambient density at a particular altitude) is assumed[11] invariant with altitude or freestream velocity v. This pressure field is fit to a multinomial $p(r,z)$ where r and z are the coordinates shown in Fig. 4.

With these assumptions, it is now possible to write the full set of coupled first-order differential equations for the bow shock region. These equations can then be numerically integrated, providing that the right-hand side of each equation is a function only of the independent variable, the dependent variables, and the first derivatives which have already been evaluated. To satisfy this condition, it is necessary to make a change of variable

$$F_i = N_i/\rho \tag{B7}$$

If this substitution is made in the chemical kinetic equations, the term $(1/\rho)(d\rho/dt)N_i$ mentioned previously is eliminated explicitly.

References

[1] Breene, R. G., Jr. and Nardone, M., "Radiant Emission from High Temperature Equilibrium Air," *Journal of Quantitative Spectroscopy and Radiative Transfer*, Vol. 2, July-Sept. 1962, pp. 272–292; also Rept. RG1SD020, May 1961, Space Sciences Div., General Electric Co., Philadelphia, Pa.

[2] Herzberg, G., *Spectra of Diatomic Molecules*, 2nd ed., Van Nostrand Reinhold, New York, 1965, p. 453.

[3] Bortner, M., "A Review of Rate Constants of Selected Reactions of Interest in Reentry Flow Fields in the Atmosphere," TN 484, May 1969, National Bureau of Standards, Washington, D.C.

[4] Baulch, D. L., Drysdale, D. D., and Horne, D. G., and Lloyd, A. C., "High Temperature Reaction Rate Data," Vol. 4, Dec. 1969 and Vol. 5, July 1970, Dept. of Physical Chemistry, Univ. of Leeds, Leeds, England.

[5] Hayes, W. D. and Probstein, R. F., *Hypersonic Flow Theory*, Vol. 1, Academic Press, New York, 1966, pp. 12–14.

[6] Gilmore, F. R., "Equilibrium Composition and Thermodynamic Properties of Air to 24000°K," RM-1543, Aug. 1955, Rand Corp., Santa Monica, Calif.

[7] Curtis, J. T. and Strom, C. R., "Computations of the Non-equilibrium Flow of a Viscous, Radiating Fluid About a Blunt Axisymmetric Body," AFFDL-TR-67-40, Vols. 1 and 2, June 1967, Cornell Aeronautical Lab., Buffalo, N.Y.

[8] Bucciero, M. and Pelech, I., private communication, April 1966, Bell Labs., Whippany, N.J.

[9] Lum, R. M. and Hines, J. N., "Telemetry System for Spherical ICBM Reentry Vehicles," *Proceedings of the National Telemetry Conference*, Inst. of Electrical and Electronic Engineers, 1970, pp. 133–138.

[10] Moore, J. A., "Chemical Non-Equilibrium in Viscous Flows," Ph.D. thesis, 1967, State Univ. of New York, Buffalo, N.Y.

[11] Evans, J. S., Schexnayder, C. J., and Huber, P. W., "Computation of Ionization in Reentry Flowfields," *AIAA Journal*, Vol. 8, No. 6, June 1970, pp. 1082–1089.